Journal of
Manufacturing and Materials Processing

MDPI

Article

Topology Optimization of Polymer-Based Bending Tools Manufactured via Additive Technology: Numerical and Experimental Validation

Luca Giorleo * and Kudret Irem Deniz

Advanced Prototyping Laboratory, Department of Mechanical and Industrial Engineering, Via Branze 38, 25123 Brescia, Italy; kudret.deniz@unibs.it
* Correspondence: luca.giorleo@unibs.it

Abstract

Sheet metal forming is a widely used manufacturing process, but the high cost and long production time of traditional forming tools limit its flexibility, especially for prototyping and small-batch production. Additive manufacturing offers a promising alternative, enabling the rapid and cost-effective fabrication of customized tools. In this study, bending tools were produced using Fused Filament Fabrication and optimized through a topology optimization approach. A combined experimental and numerical approach was applied to validate standard tool geometries and extract load conditions for use in a topology optimization process. The resulting optimized punch and die achieved a mass reduction of approximately 50% while maintaining structural integrity and safety factors well above critical thresholds. Finite Element Analysis revealed an increase in elastic deformation and stress concentration in non-critical regions, without compromising tool functionality. Experimental tests with the optimized tools confirmed their suitability for sheet metal bending, although a decrease of about 2° in the bending angle and an increase in variability were observed, consistent with simulation results. The study demonstrates the feasibility of using topology-optimized polymer tools for low-volume forming applications, offering a lightweight, cost-effective, and sustainable alternative to traditional metal tooling.

Keywords: rapid tooling; additive manufacturing; metal replacement; polymer; sheet bending

Academic Editor: Swee Hock Yeo

Received: 28 July 2025
Revised: 2 September 2025
Accepted: 5 September 2025
Published: 9 September 2025

Citation: Giorleo, L.; Deniz, K.I. Topology Optimization of Polymer-Based Bending Tools Manufactured via Additive Technology: Numerical and Experimental Validation. *J. Manuf. Mater. Process.* **2025**, *9*, 310. https://doi.org/10.3390/jmmp9090310

1. Introduction

In recent years, polymer-based tools have become a growing area of interest in sheet metal forming, especially for applications where low production volumes or prototypes are required [1,2]. Traditional forming tools, often made from tool steel or similar high-strength metals, are well-suited for large-scale production due to their durability. However, their high manufacturing costs and long lead times make them less feasible for short-run or customized operations [3]. To address these limitations, rapid tooling approaches using polymer materials have gained traction as a cost-effective and flexible alternative [4,5]. Additive manufacturing (AM), particularly Fused Filament Fabrication (FFF), allows for direct fabrication of intricate tool designs from CAD models using reinforced thermoplastics [6,7]. These advances have enabled quicker turnaround and more adaptable tooling options tailored for small-batch production needs [8,9].

Many research efforts have validated the application of AM-based polymer tools in sheet metal forming processes like bending, stamping, and deep drawing [10–13]. Even

standard thermoplastics like PLA have demonstrated sufficient capability to handle forming forces on aluminum and mild steel sheets when parameters are carefully optimized [14,15]. Moreover, fiber-reinforced polymers, including short-fiber-filled nylon and ABS composites, show enhanced mechanical and thermal properties suitable for more demanding operations [6,11,12,16]. These improvements contribute to a longer tool life, greater dimensional control, and improved surface quality, particularly when spring-back behavior is critical [17,18]. Additionally, their lower friction against metal surfaces may support dry forming and reduce or eliminate the need for lubrication [19].

Importantly, our previous study [13] demonstrated the practical feasibility of using carbon fiber-reinforced polymer tools produced via FFF in a stainless-steel V-bending application. That work showed that the printed tools could reliably form 2 mm thick steel sheets while maintaining acceptable geometry accuracy and mechanical stability over multiple cycles. Compared to unfilled polymers, the use of reinforced materials and proper print orientation contributed significantly to tool performance and repeatability. This earlier work laid the foundation for exploring new strategies to improve the structural design of polymer tools further.

Despite notable progress, limitations such as lower stiffness, elastic deformation, and reduced heat resistance still constrain the broader adoption of polymer-based tools [14,20]. These drawbacks limit their suitability in high-volume or high-temperature forming operations [16,21]. To address these issues, the current study explores the use of topology optimization as a design method to enhance both strength and material efficiency in polymer tools.

In addition to its mechanical benefits, topology optimization also contributes to sustainability by reducing the environmental impact of manufacturing. The reduction in material volume directly decreases raw material usage, energy consumption, and production time, thereby lowering the overall carbon footprint of the process. Recent studies have emphasized how optimized functional components can achieve significant mass savings while maintaining performance, which is a crucial step toward more sustainable manufacturing practices [22,23].

In this study, the authors combined both experimental and simulation-based steps. First, traditional punch and die shapes were produced using FFF and tested in a V-bending setup to understand their baseline performance. Next, finite element simulations provided contact force data, which were used to guide a topology optimization process aimed at reducing unnecessary material while maintaining tool strength. This topology optimization was chosen because it systematically redistributes the material inside the design domain according to the stress fields identified by FEM, thus maximizing stiffness and mechanical efficiency. The optimized versions were then 3D-printed and evaluated experimentally for their accuracy, structural integrity, and repeatability. These results suggest that well-designed polymer tools—enhanced through topology optimization—can offer a lightweight and effective solution for short-run metal forming, helping to extend the practical use of rapid tooling in industrial applications.

2. Materials and Methods

This section describes the geometries, materials, and processes used in the experimental campaigns, as well as the simulation setup and the methods adopted for data analysis. All phases of the research activity are summarized in Figure 1: a description of the steps followed in the research, which outlines the step-by-step workflow followed throughout the study. As shown in Figure 1, the methodology was structured into distinct steps, each of which is detailed in the following subsections.

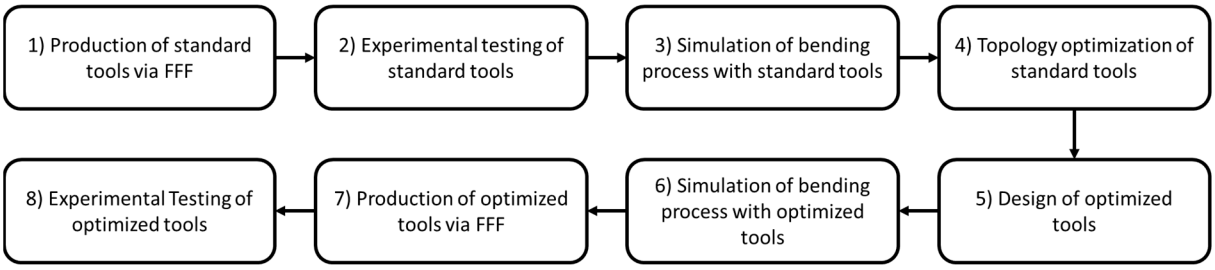

Figure 1. A description of the steps followed in the research.

Research Activity—Detailed Description

Step 1—Production of Standard Tools via FFF: The first step focused on the production of a punch and die with conventional geometry using the Fused Filament Fabrication (FFF) process. Manufacturing was carried out with a Markforged Mark Two® commercial 3D printer (Waltham, MA, USA). The technical drawings of the punch and die are shown in Figure 2a,b, respectively. The tools were oriented on the print bed so that the machine Z-axis aligned with the tool thickness, minimizing anisotropic effects in the critical direction. A 100% infill density was selected, with a 45° alternating pattern orientation. The parts were printed with two wall layers, a layer height of 0.2 mm, and a 0.4 mm brass nozzle. The material was extruded at a temperature of 260 °C, while the bed temperature was the room temperature. The material selected was Onyx, a commercial PA6 reinforced with approximately 10% to 20% by volume of short carbon fibers [24]. This material is suitable for various applications in rapid tooling for sheet metal forming, as demonstrated by the authors in previous studies [12,13].

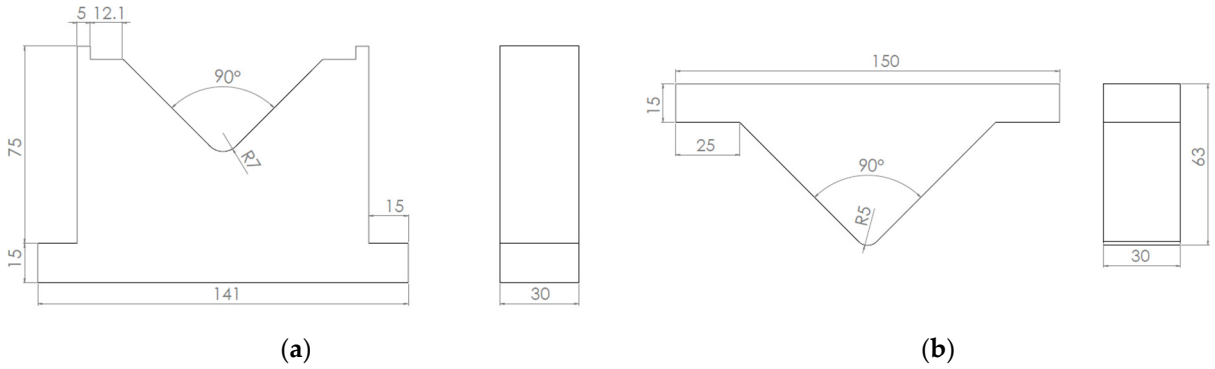

(**a**) (**b**)

Figure 2. Draft of bending die (**a**) and punch (**b**).

Step 2—Experimental Testing of Standard Tools: The metal sheets used in the forming tests were made of AISI 304 stainless steel and had dimensions of 100 × 20 × 2 mm. The mechanical properties of the materials used for both the tools (Onyx) and the sheets (AISI 304) are summarized in Table 1.

Table 1. Main mechanical properties of materials used in this research for tool (Onyx) and sheet (AISI 304) production.

	Onyx	**AISI 304**
Tensile Modulus, GPa	2.4	193
Tensile Stress at Yield, MPa	37	190
Tensile Stress at Break, MPa	40	500–700
Tensile Strain at Break, % Density, g/cm^3	25 1.2	40 8

For the experimental activity, a total of ten bending repetitions were carried out. The tools were mounted on a Galdabini RPRIC/80 industrial hydraulic press, capable of delivering up to 80 tons of force. The punch descending speed was set to 1 mm/s, while the punch stroke was adjusted to ensure 0.05 mm overbending, in order to guarantee complete contact between the punch and the sheet. Upon completion of the forming operations, geometric measurements were performed on the first, fifth, and tenth bent parts. This choice was motivated by the need to verify whether differences in bending behavior occurred at the beginning and at the end of the production lot, and to detect whether such variations emerged before or after the midpoint of the experimental sequence. Specifically, the bending angle was measured at three different locations, as shown in Figure 3a, and the thickness in the bent region was measured as indicated in Figure 3b. These measurements were obtained by scanning the sheet profile using a Renishaw Cyclone 2 coordinate measuring machine (CMM). The CMM system has an uncertainty of ±2 µm, negligible with respect to the thickness variations analyzed.

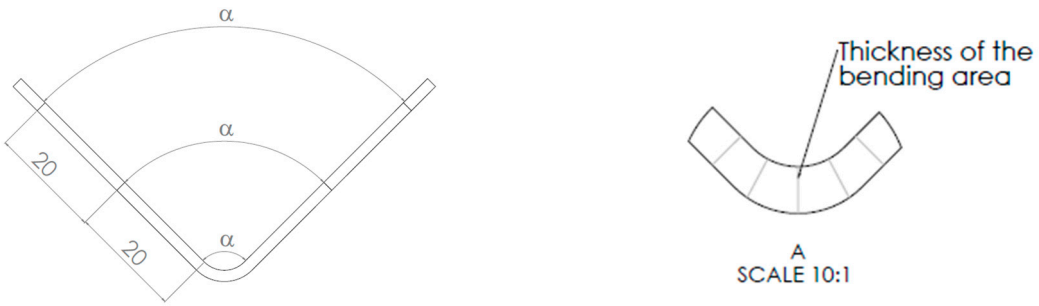

(**a**) (**b**)

Figure 3. A draft to show the methods followed for the measurement of the sheet angle (**a**) and sheet thickness evaluated in the bend area (**b**).

To assess whether the bending process induced variations in the bending angle or in the sheet thickness within the bent region as production progressed, the acquired data were analyzed using statistical tools. Specifically, a one-way ANOVA was performed to evaluate the significance of the produced sheet, and a Tukey's range test was conducted to identify differences among the tested levels.

Step 3—Simulation of the Bending Process with Standard Tools: The goal of this step was twofold: first, to assess the accuracy of the finite element model (FEM) by comparing the simulated and experimental geometries of the bent sheet; and second, to use the validated model to estimate the contact forces acting on the punch and die during the forming process. These forces, which were not directly measurable in the experimental setup, later served as input parameters for the topology optimization described in Step 4. The simulation was carried out using the commercial software DEFORM (SFTC). The mesh discretization was selected—after a preliminary screening study—to strike a balance between simulation time and result accuracy. Specifically, tetrahedral meshes were used for the punch, die, and sheet, with approximately 300,000, 40,000, and 290,000 elements, respectively. The minimum tetrahedral element size was in the range of 1 mm. A Coulomb friction coefficient of 0.2 was applied to define the contact interactions. A preliminary mesh sensitivity analysis was performed to balance accuracy and computational cost, and the adopted mesh size guaranteed stable results. Similarly, tests with friction coefficients between 0.15 and 0.25 did not significantly affect the global bending behavior; therefore, a value of 0.2 was selected as representative of the experimental setup. Figure 4 shows the meshed geometries of the punch (a), die (b), and sheet metal (c) used in the simulation model.

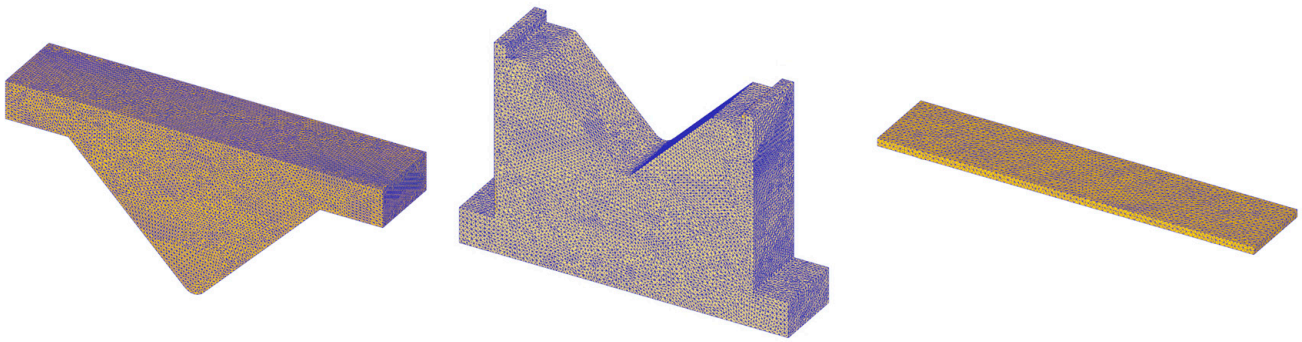

(**a**) (**b**) (**c**)

Figure 4. Punch (**a**), die (**b**) and sheet (**c**) design with relative mesh for simulation of bending process.

Once the simulation was completed, the first step was to validate its accuracy against the experimental data. To this end, the deformed geometry of the virtually bent sheet was exported from the FEM software and compared with the corresponding experimental part using Zeiss Inspect. The profiles of the bent sheets were aligned using the automatic best-fit algorithm of the Zeiss Inspect software, which minimizes the global deviation between measured and reference geometries.

Step 4—Topology Optimization of the Standard Tools: This step focused on the redesign of the punch and die through topology optimization techniques. The main settings used for the simulations are summarized in Figure 5. As shown in Figure 5a, the design space for the die is highlighted in dark red, indicating the volume available for material redistribution. The light-red regions represent areas subjected to boundary conditions (indicated by cones) and applied loads (indicated by arrows). In accordance with the experimental setup, isostatic constraints were applied at the base of the die, while three pressure loads were imposed on the working surface in contact with the sheet. The magnitude of these loads was defined based on the results from the previous simulation step. With this approach, the loads acting on the punch and die were simplified as a uniform pressure and applied to the contact surface. This assumption represents an approximation with respect to the real contact pressure distribution, which is non-uniform and varies along the bending region. However, this simplification was introduced to provide a conservative estimation of the loads and to guarantee robust optimized designs. It is worth noting that the design space was limited to the inner core of the die, maintaining an outer frame of at least 5 mm in thickness to preserve mounting and alignment integrity. The same design approach was adopted for the punch optimization, as illustrated in Figure 5b. The topology optimization was performed using Altair Inspire® 2024, setting the maximization of stiffness as the objective function. A minimum member size of 5 mm was also specified to ensure manufacturability and mechanical robustness of the resulting geometry.

Step 5–8—Post-Processing, Simulation, Manufacturing, and Experimental Testing of the Optimized Tools: Once the optimal shapes were obtained from the topology optimization, a smoothing phase was carried out to eliminate the geometric imperfections and sharp edges typical of topological solutions. This ensured both structural continuity and printability of the redesigned parts (Step 5). The smoothed geometries were then tested in a virtual environment (Step 6), using the same FEM setup and parameters as in Step 3. This allowed for a direct comparison between the performance of the standard and optimized tools under identical loading and boundary conditions. Following the numerical validation, the optimized tools were manufactured using the same FFF-based process adopted in Step 1 (Step 7). Finally, the new punch and die were employed in a bending campaign on ten AISI 304 sheets, replicating the experimental procedure and data analysis methods described in Step 2 (Step 8). The experimental results were compared with those from Step

2 by performing a two-way ANOVA, with tool design (standard and optimized) and the number of bent sheets (1st, 5th and 10th) as the investigated factors; the confidence interval was equal to 95%. In addition, a Tukey's range test was carried out.

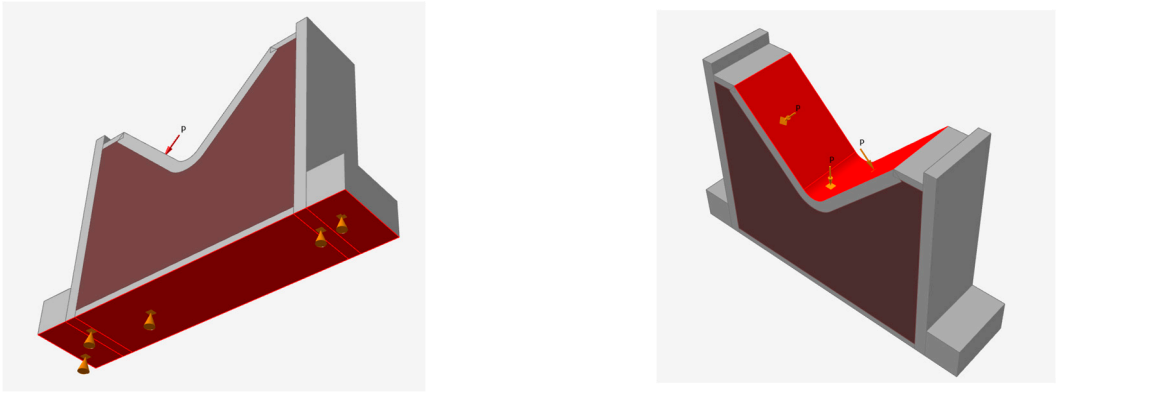

(**a**)

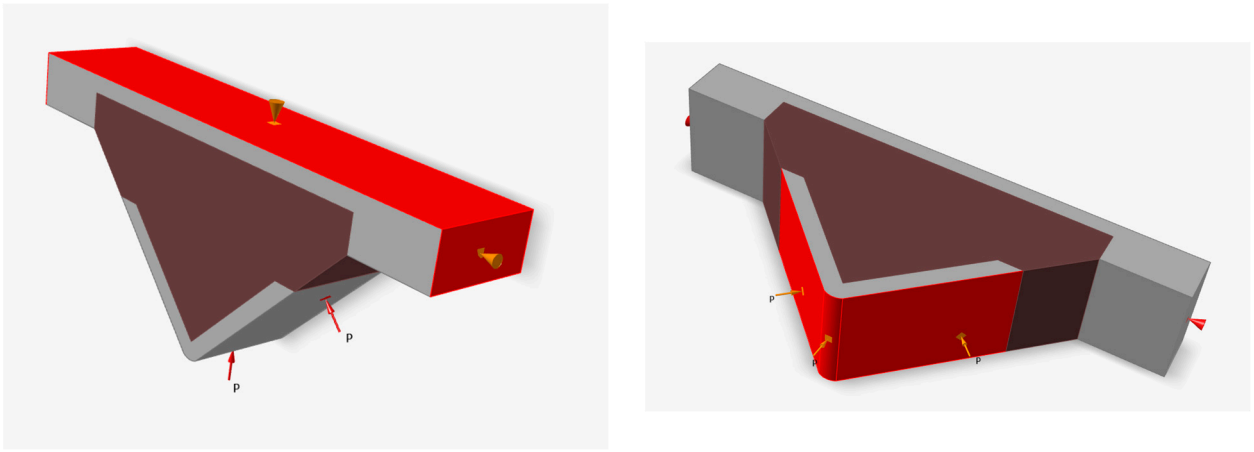

(**b**)

Figure 5. The setup adopted for the topology optimization of the die (**a**) and punch (**b**). The design space for the die is highlighted in dark red. The light-red regions represent areas subjected to boundary conditions (indicated by cones) and applied loads (indicated by arrows and P).

3. Results

This section presents the main findings of the research, structured to follow the same logical sequence used in the methodology. It begins with the experimental validation of the standard polymer tools and the numerical simulation of their behavior. Once validated, the numerical model is used to extract input data for the topology optimization process. The results of the optimization are then discussed, followed by the numerical and experimental evaluation of the performance of the optimized tools. Comparisons between standard and optimized solutions are provided to assess their feasibility, mechanical performance, and the dimensional accuracy of the bent sheets.

3.1. Experimental Standard Tool Results

To validate the repeatability and geometrical accuracy of the bending process using polymer tools with standard geometry, an experimental campaign was carried out. The results are presented and discussed below. Figure 6 presents two illustrative images from the experimental campaign carried out using tools with standard geometry: the image of the manufactured punch and die (a), and the image of the first, fifth, and tenth formed sheet metal parts (b). A visual inspection reveals no defects in the tools, either before

or after operation. As shown in Figure 6b, by overlapping the first, fifth, and tenth bent sheets, a visible angular misalignment is observed in the bending region, particularly between the first and fifth samples. The misalignment observed, particularly between the first and fifth samples, can be attributed to the progressive stabilization of the forming setup during the initial cycles. In these early operations, small adjustments in the contact interfaces, minor alignment deviations between the punch and die, and initial wear-in of the tool surfaces may occur, leading to slightly different bending responses. After these adjustments, the process stabilizes, as confirmed by the more consistent overlap observed in the tenth sample.

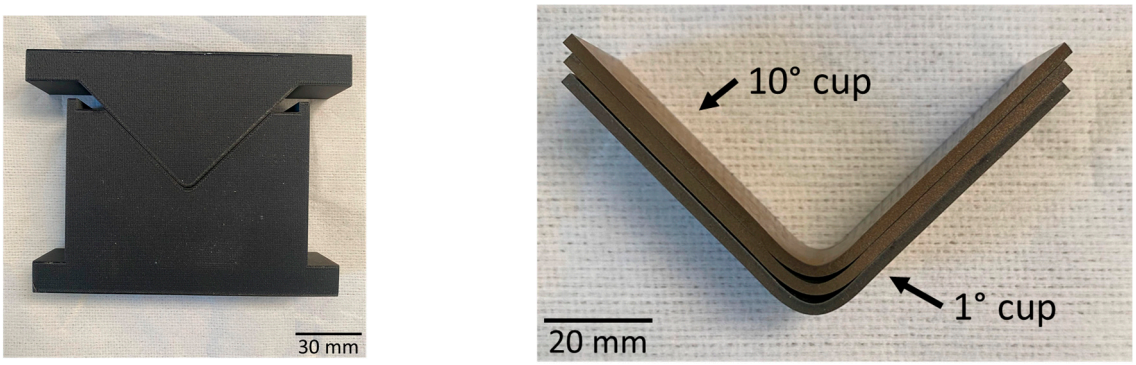

(**a**) (**b**)

Figure 6. Experimental standard tools produced (**a**); 1st, 5th, and 10th sheet produced (**b**).

The statistical analysis of the data confirm the visual inspection. The interval plot and Tukey's test results in Figure 7a confirm that the bending angle significantly differs between the first (group B) and fifth (group A) sheet (≈0.6°), while it stabilizes thereafter. In contrast, as shown in Figure 7b, the sheet thickness in the bending zone remains statistically unchanged across the production sequence (all sheets belong to the same group), indicating process stability in that dimension.

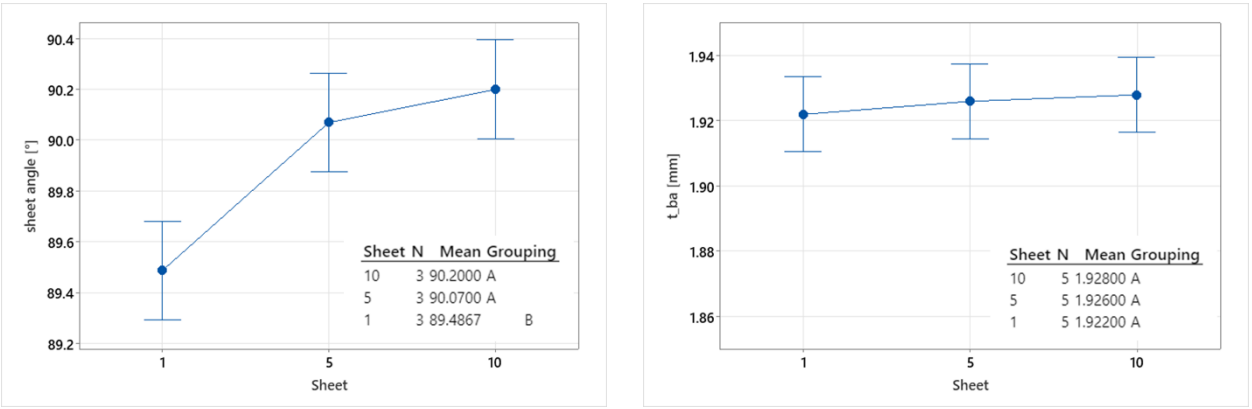

(**a**) (**b**)

Figure 7. Interval plot and Tukey's test results for the standard sheet angle (**a**) and thickness of the bending area (**b**).

Figure 8 shows the deviation map between the CAD model and the first bent sheet. Most of the geometry lies within ±0.4 mm, except for the bending zone, where deviation is attributed to angular variation. The localized overestimation in thickness (red zone) is an artifact caused by alignment errors during the inspection setup, rather than a physical change in material thickness.

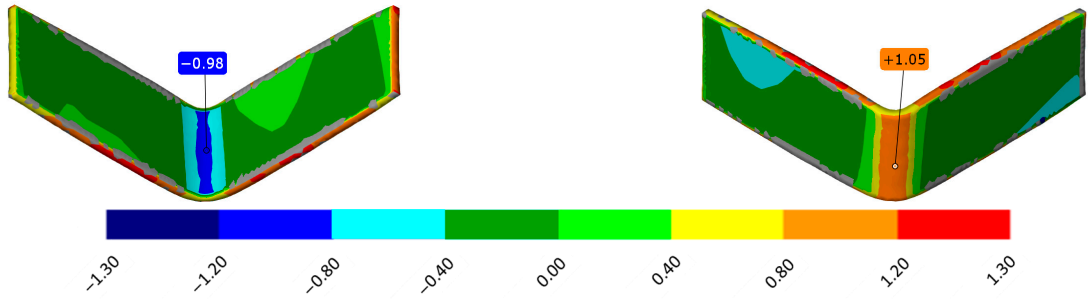

Figure 8. Front and rear false color map of deviation between first sheet bended with standard tool and CAD. Scale bar in mm.

In conclusion, the standard polymer tools demonstrated good accuracy and repeatability in producing bent sheets, with angular deviations stabilizing after the initial forming cycles. Thickness remained consistent, as expected. These results validate the feasibility of using polymer tools for low-run production and serve as a baseline for numerical comparison in the following sections.

3.2. Numerical Standard Tool Results

Figure 9 shows the deviation map obtained by comparing the FEM-predicted geometry with the experimental result from the first bent sheet. As shown, the majority of the surface lies within a ± 0.5 mm tolerance band, with slightly higher deviations localized in the bending zone. This outcome confirms the good predictive capability of the numerical model in replicating the real deformation behavior of the sheet, thus validating its use for further process investigation.

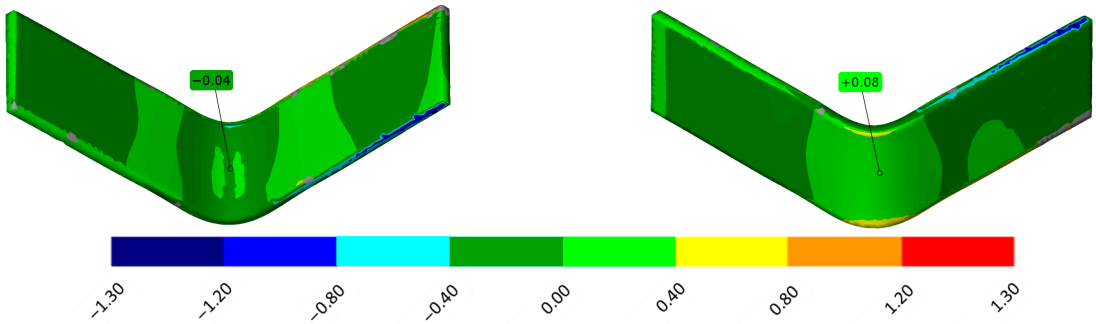

Figure 9. Front and rear false color map of deviation between first sheet bended with standard tool and FEM. Scale bar in mm.

After validating the model, the simulation was used to extract the contact forces acting on the forming tools. Figure 10 shows the distribution of contact forces acting on the punch and die surfaces during the forming phase, as obtained from the FEM simulation. The normal force on the punch surface ranges from a minimum of approximately 300 N up to a peak of 2600 N. The highest concentration of force is observed at the bending radius of the punch, particularly in the mid-plane region, where the material flow is most constrained. This localized pressure is consistent with the area where maximum plastic deformation occurs in the sheet. On the die side, the force distribution is more uniform along the contact surface, but slightly higher values are registered in the entry zone of the die shoulder, where the sheet initially makes contact and starts to wrap around the geometry. The force decreases progressively along the die flanks, suggesting a gradual release of contact pressure as the sheet flows through the forming cavity.

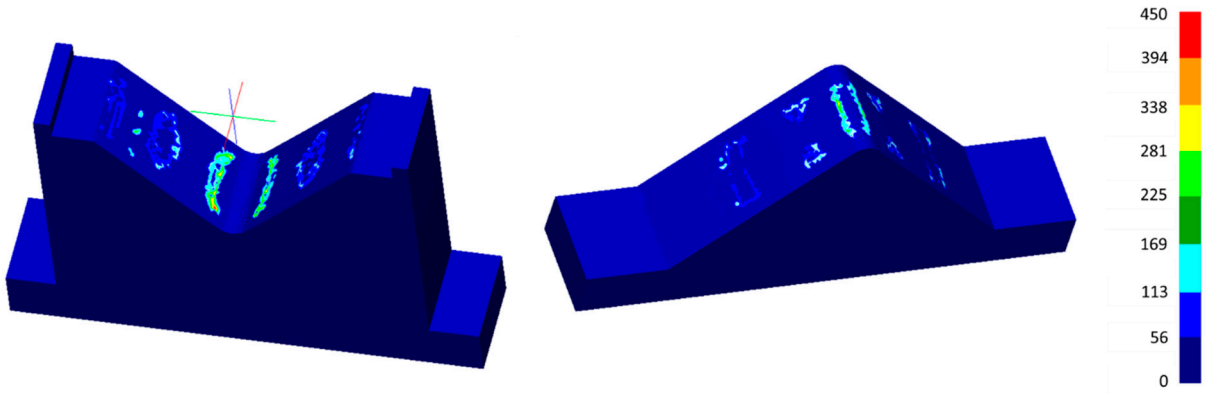

Figure 10. False color map of bending load acting on the standard die (**left**) and on the punch (**right**). Scale bar in daN.

This detailed force map not only highlights the critical load-bearing zones on both tools, but also provides a reliable estimation of the pressure field to be used as an input for the topological optimization of the punch geometry presented in Section 3.3.

3.3. Topology Optimization of Standard Tool and FEM Results

This section presents the results of the topology optimization performed on the conventional punch and die geometries. The design conditions—namely loads, constraints, and design space—were defined in Section 2, under the description of Step 3, with the exception of the input pressure value, which was specifically determined through the FEM analysis conducted on the standard tools. To adopt a conservative design approach, a constant pressure corresponding to the maximum measured forming force was applied. From the previous FEM analysis, the peak punch force was found to be 2600 N. By assuming an application area of 100 mm^2, the resulting input pressure was set to 26 MPa. The contact area was estimated based on the regions of highest stress concentration observed in the FEM results. These were located in the central portion of the punch, roughly matching the sheet width of 20 mm and extending about 5 mm along the punch profile. Based on these assumptions, the topology-optimized geometries of the punch and die were computed and are shown in Figure 11. Analyzing Figure 11, it can be observed that the optimization software concentrates most of the material in the die around the bending angle area, where the stress concentration is highest during forming. In contrast, for the punch, the algorithm suggests reinforcing the peripheral regions adjacent to the contact zone with the sheet metal—areas that were intentionally excluded from the design space. This outcome confirms the model's tendency to allocate material outside the deforming interface, thereby preserving structural integrity while minimizing mass.

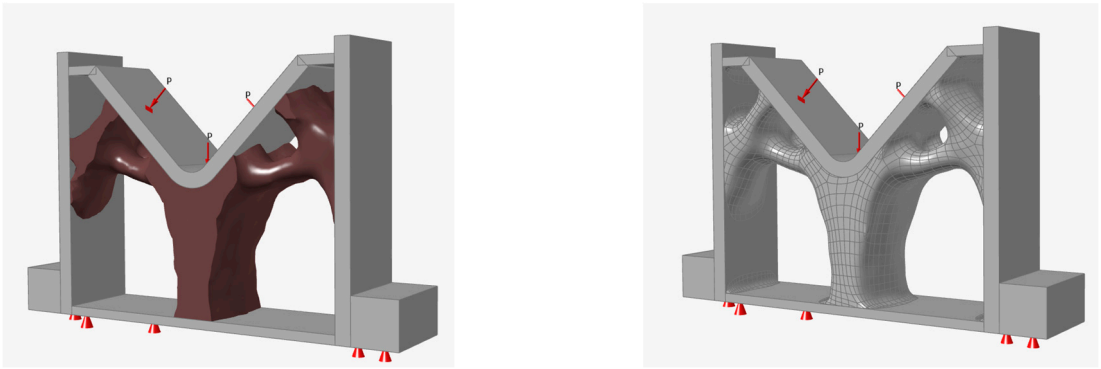

(**a**)

Figure 11. *Cont.*

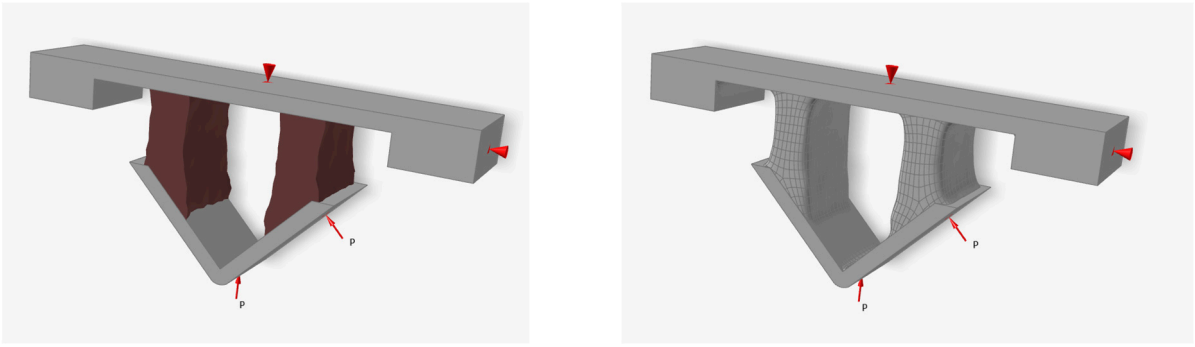

(**b**)

Figure 11. The new tools' geometry, obtained from topology optimization analysis for bending the die (**a**) and punch (**b**). On the left, the geometry as designed, and on the right, the geometry after the smoothing process.

Table 2 summarizes the main differences between the standard and topology-optimized geometries. The results show that the optimization process led to a significant mass reduction, with both the punch and the die reaching approximately 50% of their initial mass. This weight reduction, however, resulted in a decrease in the safety factor—defined as the ratio between the material yield strength and the maximum equivalent stress developed during the operation. Specifically, the safety factor decreased by 22% for the die and by 79% for the punch. Despite this reduction, the final safety factors—7.0 for the die and 13.2 for the punch—are still largely sufficient to ensure safe and reliable operation of the tools under the prescribed loading conditions. Another noteworthy variation is in the average displacement of the tools during the forming process, which increased by 70% for the die and by 274% for the punch. However, it is important to emphasize that the absolute values of displacement remain in the order of hundredths of a millimeter, i.e., at least three orders of magnitude smaller than the overall tool dimensions, which are in the range of several hundred millimeters. Therefore, these deformations are negligible in practical terms and do not compromise process accuracy. Finally, the maximum stress in the optimized tools reached 5.7 MPa in the die and 3.0 MPa in the punch. As reported in Table 1, the yield strength of the composite material used is 37 MPa, indicating that the stresses remain well below the critical limit and well within the elastic regime.

Table 2. Comparison of mechanical characteristics between standard and optimized tool geometries.

Tool	Parameter	Standard	Optimized	Gain/Loss (%)
Die	Safety Factor	9	7	−22%
	Weight [kg]	0.303	0.15	−50%
	Max. Displacement [mm]	6.70×10^{-2}	1.14×10^{-1}	70%
	Max. Stress [MPa]	4.4	5.7	30%
Punch	Safety Factor	64	13.2	−79%
	Weight [kg]	0.171	0.09	−47%
	Max. Displacement [mm]	9.16×10^{-3}	3.43×10^{-2}	274%
	Max. Stress [MPa]	0.625	3.04	386%

3.4. Numerical Optimized Tool Results and Comparison with Standard Tools

Once the lightweight geometries were obtained through topology optimization, the performance of the tools was tested in a virtual environment to evaluate the potential differences in the bending process. Figure 12 shows the accumulated displacement in the Z-direction experienced by the sheet during bending. The comparison reveals that the sheet formed using the optimized tools exhibits lower Z-displacement, indicating that it

underwent less deformation during the process. Given that the simulations were performed under identical conditions—particularly with the same punch stroke—this variation is likely attributable to tool deformation during forming. In particular, the lower stiffness of the optimized punch and/or die may have led to elastic deflection, thereby reducing the effective force transmitted to the sheet and thus its resulting deformation.

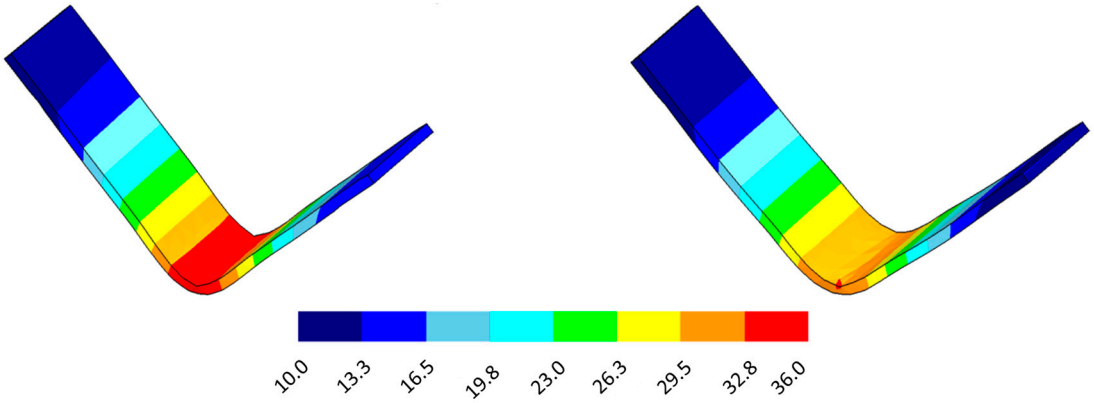

Figure 12. FEM Z-displacement evaluated for sheet bended with standard tools (**left**) and optimized tool (**right**). Scale bar in mm.

This hypothesis is confirmed by the Z-displacement maps of the forming tools themselves, as shown in Figure 13. In Figure 13a, the optimized punch exhibits a maximum Z-displacement of 2.3 mm on the bending angle, compared to 0.7 mm for the standard punch. Similarly, in Figure 13b, the optimized die shows a Z-displacement of 0.3 mm, whereas the standard die deforms by only 0.05 mm. Although these values represent a clear increase in elastic deformation, they remain in the order of tenths to hundredths of a millimeter, and are therefore negligible with respect to the overall tool dimensions (typically in the range of 100–200 mm). These displacements do not compromise the functionality or dimensional accuracy of the formed sheets. However it is possible to observe a difference when comparing the displacement calculated by Inspire software reported in Table 2 and the results shown in Figure 13; to clarify this difference, it is important to note that the displacement values obtained from Inspire during topology optimization are calculated with a quasi-static approach and are mainly useful for relative comparison, while Defotm simulations employ a plasticity-based solver and provide results that better reflect the actual forming process.

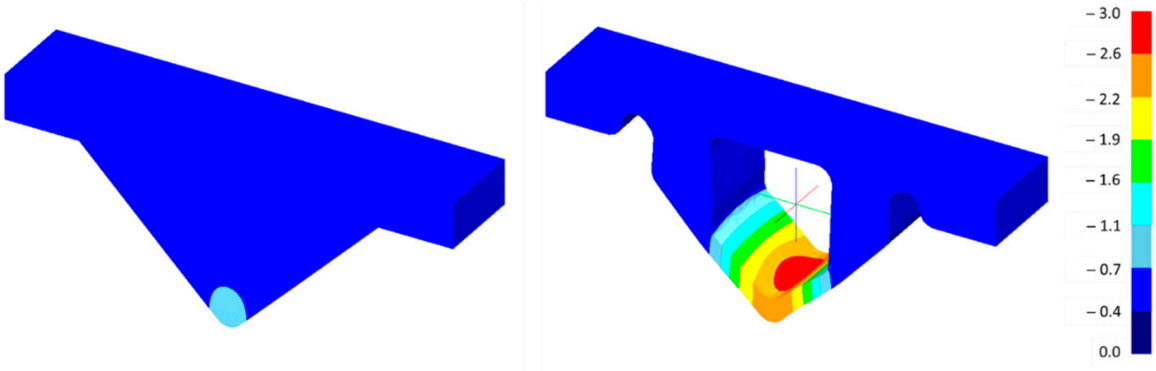

(**a**)

Figure 13. *Cont.*

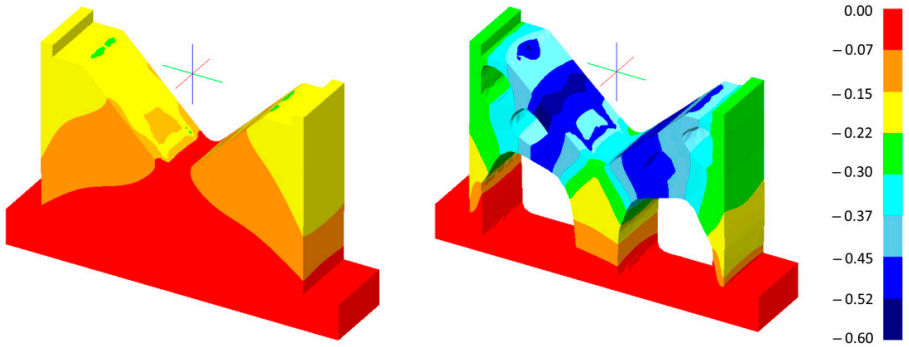

(**b**)

Figure 13. Comparison of Z-displacement between standard (**left**) and optimized (**right**) punch (**a**) and die (**b**). Scale bar in mm.

In addition to the displacements, the effective stress fields developed during the bending process were also analyzed to evaluate how material redistribution affects load transmission. As shown in Figure 14, the maximum stress in the optimized punch (Figure 14a) remains comparable to that of the standard version; however, the stress distribution changes significantly. In particular, the regions adjacent to the bending area become more involved in carrying the load, exhibiting higher stress levels. This behavior is also observed in the die (Figure 14b), where the load is distributed across a broader area in the optimized geometry compared to the standard one.

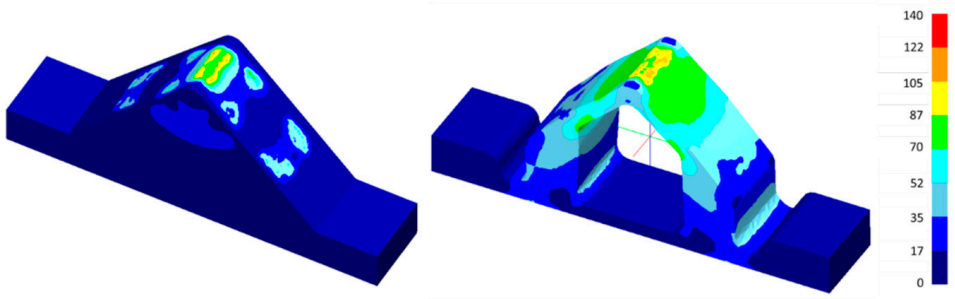

(**a**)

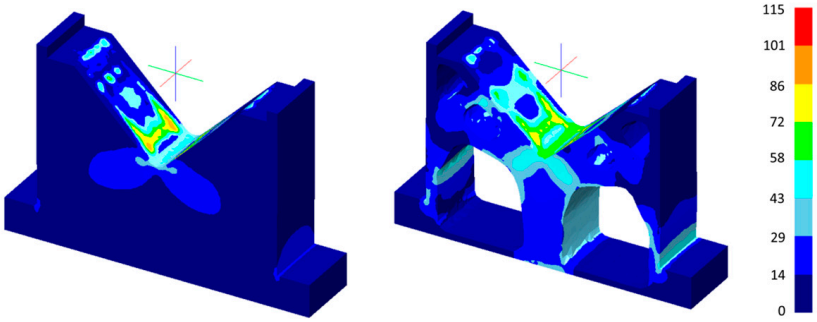

(**b**)

Figure 14. Effective stress evaluated on standard (**left**) and optimized (**right**) punch (**a**) and die (**b**). Scale bar in MPa.

Overall, the numerical simulations show that the topologically optimized tools are capable of maintaining performance levels comparable to those of the standard tools in terms of part geometry, while achieving significant mass reduction and operating within acceptable safety margins.

3.5. Experimental Optimized Tool Results and Comparison with Standard

This section presents the results of the experimental campaign conducted using the topology-optimized forming tools, which are shown in Figure 15a. The first, fifth, and tenth bent sheets produced with these tools are illustrated in Figure 15b. A visual inspection of the tools carried out after the bending operations confirmed the absence of defects, fractures, or permanent deformations. The tools maintained their structural integrity throughout the forming sequence, indicating that the optimized geometries are mechanically robust and suitable for repeated use under the tested conditions.

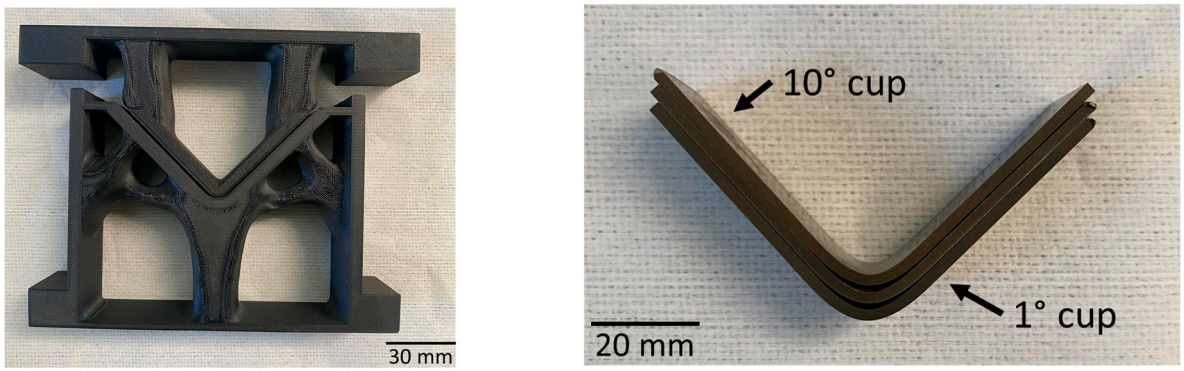

(**a**) (**b**)

Figure 15. Experimental optimized tools produced (**a**); 1st, 5th, and 10th sheet produced (**b**).

The statistical analysis concerning the bending angle and sheet thickness in the bent region is shown in Figure 16.

Source	DF	Adj SS	Adj MS	F-Value	P-Value
Tool Geometry	1	15.1250	15.1250	172.39	0.000
Sheet	2	0.7795	0.3898	4.44	0.036
Tool Geometry*Sheet	2	0.1937	0.0969	1.10	0.363
Error	12	1.0529	0.0877		
Total	17	17.1511			

Source	DF	Adj SS	Adj MS	F-Value	P-Value
Tool Geometry	1	0.112853	0.112853	331.92	0.000
Sheet	2	0.000407	0.000203	0.60	0.558
Tool Geometry*Sheet	2	0.000047	0.000023	0.07	0.934
Error	24	0.008160	0.000340		
Total	29	0.121467			

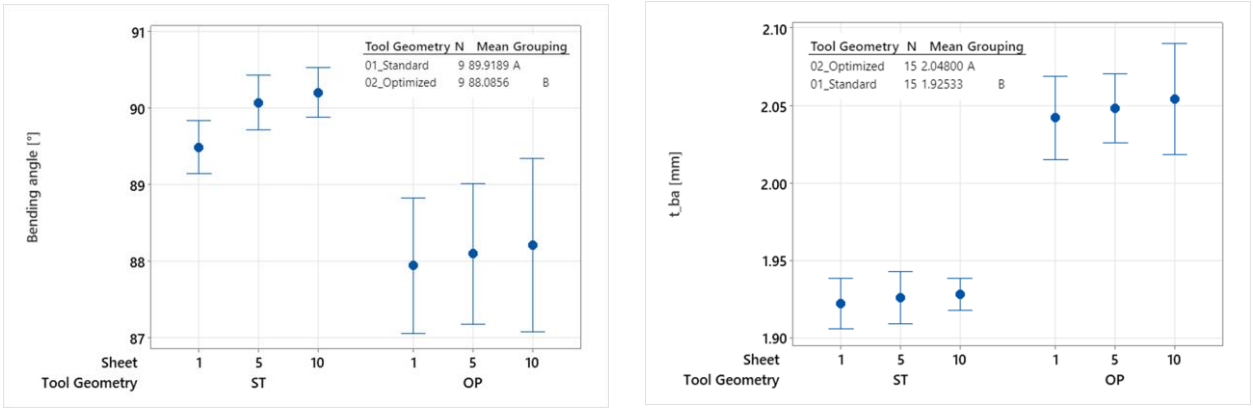

(**a**) (**b**)

Figure 16. Interval plot and Tukey's test results for standard and optimized sheet angle (**a**) and thickness of bending area (**b**). ST for standard tools and OP for optimized.

The ANOVA performed on the bending angle measurements (sheet angle) revealed a statistically significant effect of the tool geometry (i.e., optimized vs. standard tools), while the number of bent sheets did not show any significant influence. This outcome was confirmed by Tukey's post hoc test. As highlighted in the interval plot (Figure 16a),

the sheets produced with the topology-optimized tools exhibit a mean bending angle approximately 2° lower than those formed with conventional tools. This difference can be attributed—consistent with the FEM results discussed in the previous section—to the elastic deformation of the optimized tools, which leads to a lower effective Z-displacement during the forming process, thereby slightly reducing the achieved bending angle. Moreover, the sheets formed using the optimized tools show greater variability in the bending angle. This increased dispersion is due to non-uniform bending across the sheet width, which results in different angle values at the three measurement locations (see Figure 3a). This behavior is supported by the displacement map of the optimized die (Figure 13b), which shows variation in Z-displacement along the contact profile where the sheet rests during forming—leading to uneven force transmission and thus a more scattered bending response. Further evidence of this phenomenon is provided in Figure 17, which displays a color deviation map comparing sheets bent with optimized tools to those bent with standard tools. The figure highlights not only a systematic reduction in the bending angle, but also noticeable deviation in the undeformed sheet region, suggesting slight shifts or rotations during the process. The differences in absolute values observed between the statistical results and the color map are mainly due to the resolution limits of the different measurement methods used.

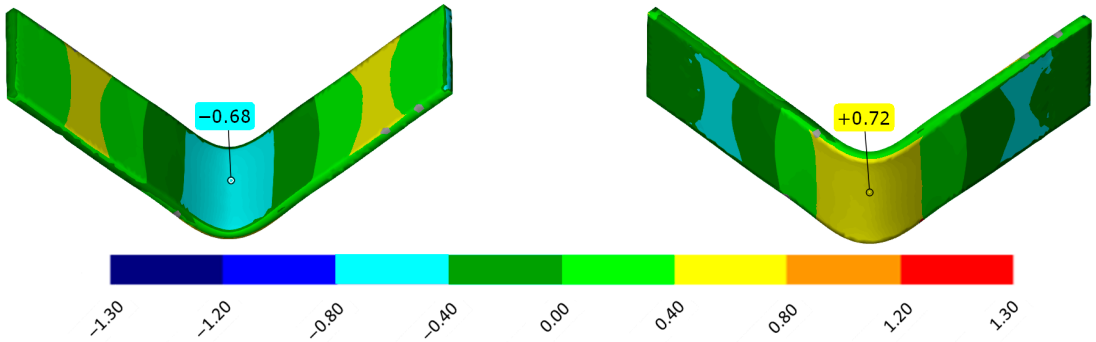

Figure 17. Front and rear false color map of deviation between first sheet bent with standard and optimized tools. Scale bar in mm.

The analysis of sheet thickness in the bending zone, presented in Figure 16b, shows that—similarly to the bending angle—the number of produced sheets does not significantly affect the outcome, whereas the type of tool used does. In particular, sheets formed with topology-optimized tools exhibit a smaller thickness reduction in the bent region compared to those formed with conventional tools. This behavior can again be explained by the lower stiffness of the optimized punch and die, which offer less resistance to the forming loads. As a result, the sheet undergoes slightly less severe bending, reducing the typical tensile–compressive stress gradient that leads to thinning in the bending zone. In other words, a lower effective bending angle leads to less material stretch, and thus a smaller reduction in thickness.

4. Conclusions

This study investigated the use of topology optimization for polymer-based bending tools manufactured via additive technology. The main findings can be summarized as follows:

- Feasibility of polymer tools: Standard polymer tools produced by FFF showed good repeatability and accuracy in sheet bending operations, with no evidence of wear or failure after multiple cycles.

- Mass reduction: The topology-optimized punch and die achieved a weight reduction of about 50% compared to standard geometries.
- Structural performance: Despite reduced safety factors (down to 7.0 for the die and 13.2 for the punch), both tools remained well within safe operational limits.
- Experimental confirmation: The optimized tools maintained structural integrity during bending tests; however, the sheets bent by the optimal tools showed a lower mean bending angle ($\approx 2^\circ$ decrease) and greater variability compared to those bent with the standard tools. Nevertheless, it should be noted that the reduction of about 2° in the bending angle observed with the optimized tools can be easily compensated for in industrial practice by slightly increasing the punch stroke. Therefore, this difference does not represent an operational limitation, but rather a minor adjustment in the process setup.
- Sustainability potential: The combination of additive manufacturing and topology optimization provides a lightweight and material-efficient solution, which is particularly suitable for low-volume or prototype production.

Future work will extend this approach to multi-step forming processes, investigate long-term wear behavior, and explore different load scenarios to refine the reliability of optimized polymer tools.

Author Contributions: Conceptualization, L.G.; methodology, L.G.; validation, L.G.; investigation, L.G.; data curation, L.G. and K.I.D.; writing—original draft preparation, L.G. and K.I.D.; writing—review and editing, L.G. and K.I.D.; supervision, L.G. All authors have read and agreed to the published version of the manuscript.

Funding: This research received no external funding.

Data Availability Statement: The data presented in this study are available on request from the corresponding author.

Acknowledgments: The authors are grateful to R. Pinti of Pinti Inox S.p.a.—Sarezzo (Brescia) for providing support in the experimental campaign and the CMM analysis.

Conflicts of Interest: The authors declare no conflicts of interest.

References

1. Cooper, D.R.; Rossie, K.E.; Gutowski, T.G. The energy requirements and environmental impacts of sheet metal forming: An analysis of five forming processes. *J. Mater. Process. Technol.* **2010**, *244*, 116–135. [CrossRef]
2. Müller, H.; Sladojevic, J. Rapid tooling approaches for small lot production of sheet-metal parts. *J. Mater. Process. Technol.* **2001**, *115*, 97–103. [CrossRef]
3. Merklein, M.; Lechner, M.; Kuppert, A. A review on tailored blanks—Production, applications and evaluation. *CIRP Ann.* **2014**, *63*, 595–612. [CrossRef]
4. Ngo, T.D.; Kashani, A.; Imbalzano, G.; Nguyen, K.T.Q.; Hui, D. Additive manufacturing (3D printing): A review of materials, methods, applications and challenges. *Compos. Part B Eng.* **2018**, *143*, 172–196. [CrossRef]
5. Schuh, G.; Bergweiler, G.; Bickendorf, P.; Fiedler, F.; Colag, C. Sheet metal forming using additively manufactured polymer tools. *Procedia CIRP* **2020**, *93*, 20–25. [CrossRef]
6. Torrado, A.R.; Shemelya, C.M.; English, J.D.; Lin, Y.; Wicker, R.B.; Roberson, D.A. Characterizing the effect of additives to ABS on the mechanical property anisotropy of specimens fabricated by material extrusion 3D printing. *Addit. Manuf.* **2015**, *6*, 16–29. [CrossRef]
7. Tekinalp, H.L.; Kunc, V.; Velez-Garcia, G.M.; Duty, C.E.; Love, L.J.; Naskar, A.K.; Blue, C.A.; Ozcan, S. Highly oriented carbon fiber–polymer composites via additive manufacturing. *Compos. Sci. Technol.* **2014**, *105*, 144–150. [CrossRef]
8. Tymrak, B.M.; Kreiger, M.; Pearce, J.M. Mechanical properties of components fabricated with open-source 3D printers under realistic environmental conditions. *Mater. Des.* **2014**, *58*, 242–246. [CrossRef]
9. Tondini, F.; Basso, A.; Arinbjarnar, U.; Nielsen, C.V. The performance of 3D printed polymer tools in sheet metal forming. *Metals* **2021**, *11*, 1256. [CrossRef]

10. Szalai, S.; Szívós, B.F.; Nemes, V.; Szabó, G.; Kurhan, D.; Sysyn, M.; Fischer, S. Investigation of FDM-Based 3D Printing for Optimized Tooling in Automotive and Electronics Sheet Metal Cutting. *Appl. Sci.* **2025**, *15*, 442. [CrossRef]
11. Zaragoza, V.G.; Strano, M.; Iorio, L.; Monno, M. Sheet metal bending with flexible tools. *Procedia Manuf.* **2019**, *29*, 232–239. [CrossRef]
12. Giorleo, L.; Ceretti, E. Aluminium deep drawing with additive manufacturing polymer punches: Analysis of performance in small batch production. *Int. J. Adv. Manuf. Technol.* **2023**, *128*, 2175–2185. [CrossRef]
13. Giorleo, L.; Deniz, K.I. Polymer Tools Produced by Fused Filament Fabrication for Steel-Bending Process: Effect of Layering Orientation. *J. Manuf. Mater. Process.* **2024**, *8*, 243. [CrossRef]
14. Trzepieciński, T. Recent developments and trends in sheet metal forming. *Metals* **2020**, *10*, 779. [CrossRef]
15. Jagadeesha, T.; Kunar, S. Integrating Metal Forming and Additive Manufacturing for Enhanced Product Quality and Efficiency. In *Advances in Additive Manufacturing*; Wiley: Hoboken, NJ, USA, 2024; pp. 129–143. [CrossRef]
16. Geueke, M.; Frohn-Sörensen, P.; Reuter, J.; Padavu, N.; Reinicke, T.; Engel, B. Structural optimization of additively manufactured polymer tools for flexible sheet metal forming. *Procedia CIRP* **2021**, *104*, 1345–1350. [CrossRef]
17. Kaleem, M.A.; Steinheimer, R.; Frohn-Sörensen, P.; Kotzian, T.; Engel, B. Topology optimization of forming tools: Pressure die in rotary draw bending process. *Int. J. Interact. Des. Manuf.* **2025**, *19*, 3349–3362. [CrossRef]
18. Wang, H.; Xie, H.; Liu, Q.; Shen, Y.; Wang, P.; Zhao, L. Structural topology optimization of a stamping die made from high-strength steel sheet metal based on load mapping. *Struct. Multidiscip. Optim.* **2018**, *58*, 769–784. [CrossRef]
19. Hedayati, R.; Alavi, M.; Sadighi, M. Effect of degradation of polylactic acid (PLA) on dynamic mechanical response of 3D printed lattice structures. *Materials* **2024**, *17*, 3674. [CrossRef] [PubMed]
20. Dogan, O. Short-term creep behaviour of different polymers used in additive manufacturing under different thermal and loading conditions. *Stroj. Vestn.-J. Mech. Eng.* **2022**, *68*, 451–460. [CrossRef]
21. Sivakumar, N.K.; Palaniyappan, S.; Basavarajappa, S.; Hashem, M.I.; Bodaghi, M.; Sekar, V. Study on the impact of material extrusion factors on the compressive characteristics of honeycomb lattice-structured Onyx™ composites. *Mater. Today Commun.* **2023**, *37*, 107317. [CrossRef]
22. Almonti, D.; Salvi, D.; Mingione, E.; Vesco, S. Lightweight and Sustainable Steering Knuckle via Topology Optimization and Rapid Investment Casting. *J. Manuf. Mater. Process.* **2025**, *9*, 252. [CrossRef]
23. Bajpai, R.P.; Chandrasekhar, U.; Arankalle, A.R. *Innovative Design and Development Practices in Aerospace and Automotive Engineering*; Springer: Singapore, 2017.
24. Nikiema, D.; Balland, P.; Sergent, A. Study of the mechanical properties of 3D-printed onyx parts: Investigation on printing parameters and effect of humidity. *Chin. J. Mech. Eng. Addit. Manuf. Front.* **2023**, *2*, 100075. [CrossRef]